

High-Resolution Measurements of Auger-Electron and Photoelectron Structure in the Secondary-Electron Energy Distributions of Aluminum, Nickel, and Copper*

C. J. Powell and A. Mandl†

National Bureau of Standards, Washington, D. C. 20234

(Received 19 June 1972)

Measurements are reported of selected structure in the secondary-electron energy distributions of evaporated aluminum, nickel, and copper. The specimens were bombarded with 3-keV electrons and the secondary structure was measured with a resolution of 0.1 eV. For each metal, it was hoped to measure Auger transitions involving two relatively narrow inner-shell levels and the valence band in order to obtain information on the valence-band density of states. Attempts were made to observe the Al $KL_{2,3}M$ Auger-electron energy distribution expected at about 1470 eV. Structure was, however, observed with a high-energy edge of 1485.9 ± 0.5 eV and a breadth of 8–9 eV. This structure was interpreted as being due to photoemission of valence electrons by internally generated $K\alpha$ x rays and was similar to uv photoelectron energy distributions and to the calculated density of states. Inelastic scattering of the photoelectrons obscures the expected Al $KL_{2,3}M$ structure. Auger-electron peaks in the ranges 730–800 and 820–865 eV were measured in the secondary-electron energy spectra for nickel and copper, respectively. Structure was observed in the $L_3M_{2,3}M_{4,5}$ Auger transition (over a range of about 20 eV) that could be associated in part with the final atomic states and in part with over-all features of the $3d$ -band density of states as determined by soft-x-ray-emission spectroscopy and x-ray photoelectron spectroscopy. It is believed that Auger-electron spectra can yield useful data on changes of electronic structure (e.g., by alloying or by compounding) but, in general, density-of-states data cannot be derived from the Auger spectra without detailed knowledge of the final states expected after the Auger transition of interest.

I. INTRODUCTION

It has long been realized that features in the secondary-electron energy distributions of solids (excited by electron impact) can give information on the electronic structure of the solid. Two types of measurement have usually been made. First, measurements of electron energy-loss spectra (due to excitation of both valence¹ and inner-shell² electrons) can be analyzed to yield optical constants³ and thus be related to band structure.⁴ Second, measurements of Auger-electron transitions involving valence-band electrons can be related to the valence-electron density of states $N(E)$.^{5,6}

One of the original objectives of the work to be described here was to deduce density-of-states data from suitable Auger peaks in the secondary-electron energy distributions of selected solids, as suggested by Lander.⁵ Earlier work of this type has been restricted to K valence-valence Auger transitions^{6(a),6(c),6(e)} or to L valence-valence Auger transitions.^{6(b),6(d)} For such transitions, the observed Auger-electron energy distributions would be proportional to an integral self-convolution of the density of states times the transition probability, assuming that the final holes in the valence band do not appreciably modify $N(E)$. To avoid deconvolution of the raw spectral data, it was decided to observe Auger transitions involving two relatively well-defined inner-shell levels and the valence

band. It was hoped that density-of-states data derived in this way could be usefully compared and contrasted with the results of other techniques (uv photoemission,^{7(a)} x-ray photoemission,^{7(b)} and soft-x-ray emission spectroscopy^{7(c)}). With all of these techniques it is usually difficult to determine the energy dependence of the transition probability specific to each type of electronic transition and the effects of particular vacancies or excitations on the observed distributions. In the absence of a complete theory to describe each type of measurement, comparisons and contrasts of experimental data obtained by different methods for a given material can be valuable in determining the common features of $N(E)$, the energy variation of the several transition probabilities, and the importance of specific initial- or final-state effects on the different spectral distributions.

Aluminum, nickel, and copper were selected for measurement in this work. Aluminum is a nearly-free-electron low- Z metal and it was believed that a measurement of the Al $KL_{2,3}M$ Auger transition for a metal with such a relatively simple electronic structure would provide a good test of the usefulness of the Auger technique for deriving $N(E)$ information. Nickel and copper have a more complex electronic structure that has been investigated with the use of other techniques⁷ so that comparisons of results are readily possible. The $L_3M_{2,3}M_{4,5}$ and $L_3M_{2,3}N_1$ transitions were selected as being useful

TABLE I. Ground-state binding energies of electrons (taken from Ref. 8) and the widths W_K , W_{L_3} , and W_{M_3} of the K , L_3 , and M_3 levels, respectively (taken from Refs. 9 and 10), of Al, Ni, and Cu (all in eV).

	Al	Ni	Cu
Binding energies			
K	1559.6	8332.8	8978.9
L_1	117.7	1008.1	1096.1
L_2	73.1	871.9	951.0
L_3		854.7	931.1
M_1		111.8	119.8
$M_{2,3}$		68.1	73.6
Level widths			
W_K	~ 0.3		
W_{L_3}	~ 0.1	~ 0.5	0.5
W_{M_3}		0.2–0.4	0.2–0.4

for each metal and convenient to measure; these transitions could give information on the $3d$ - and $4s$ -electron contributions, respectively, to the valence band. Nickel and copper are also neighboring elements in the Periodic Table, nickel being the last element of the first transition series and copper a noble metal, so that any differences in their Auger spectra could possibly indicate how the transition features change with the filling of the $3d$ level. Table I lists the binding energies of electrons⁸ involved in the selected transitions as well as the widths of the K , L_3 and M_3 levels.^{9,10} The level widths set a natural limit to the resolution with which valence-band features in the various Auger transitions can be measured (unless deconvolution techniques are employed). In the present work, it was decided to measure the selected features with an analyzer resolution of 0.1 eV so that the over-all energy resolution of the valence-band structure was not appreciably inferior to that ex-

pected from the relevant inner-shell level widths.

The apparatus and the methods of data accumulation and analysis will be described in Sec. II. Results for aluminum and for nickel and copper will be separately presented and discussed in Secs. III and IV, respectively.

II. EXPERIMENTAL

Figure 1 shows a schematic outline of the apparatus used in this work. Specimens were prepared by evaporation from tungsten helical filaments in the case of Al and from tungsten conical baskets in the case of Ni and Cu. The maximum pressure during the 5–10-sec evaporation was usually between 5 and 10×10^{-9} Torr, while the base pressure was between 1 and 3×10^{-9} Torr.

The electron gun used to produce the 3-keV primary beam consisted of a Pierce diode¹¹ and a single focusing element with deflection plates. Features of the secondary-electron energy distribution were measured with a Kuyatt–Simpson analyzer system¹² operated with a resolution of 0.1 eV, independent of the absolute electron energy being measured.¹³

Electrons enter the analyzer system through two 0.014-in.-diam molybdenum apertures spaced 0.125 in. apart; the distance between the center of the target and the nearest aperture is 1 in. These electrons are decelerated and then dispersed in the electrostatic field between two concentric hemispheres. The beam transmitted through the energy-defining aperture is reaccelerated and detected with an electron multiplier. Copper was used for the fabrication of the analyzer hemispheres and all lens elements. The earth's magnetic field was neutralized (to about 2 mG) over the experimental volume with two pairs of rectangular coils.¹⁴ The effects of residual fields and of small mechanical misalignments could be corrected by use of

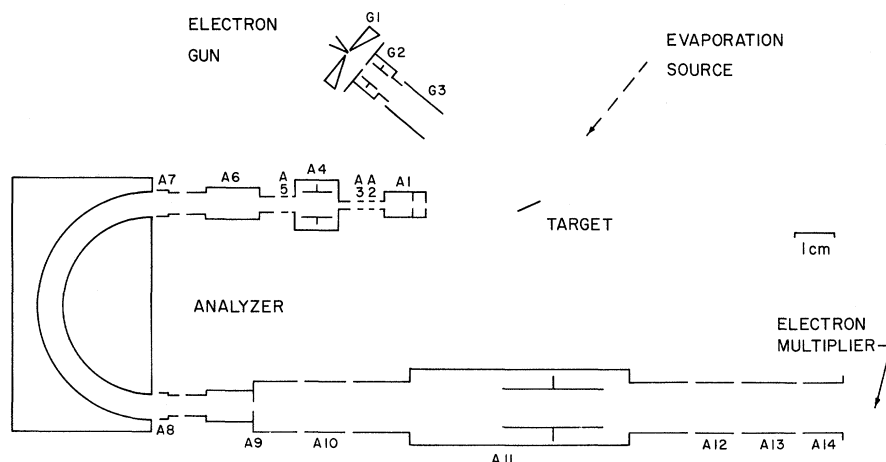


FIG. 1. Schematic outline of the apparatus. The gaps between the electrodes have been enlarged for clarity.

two pairs of deflection plates in each linear segment of the apparatus.

Output pulses from the electron multiplier were counted and stored in a multichannel analyzer, operated in the multiscale mode. A staircase waveform was produced by the multichannel analyzer as it moved from channel to channel; this waveform was amplified and applied to the scattering apparatus to provide an energy sweep of variable amplitude. Data accumulated in the multichannel analyzer could be punched on paper tape for later computer processing (e.g., summing of runs on a common energy scale).

The apparatus was used to search for and to measure Auger-electron features in the secondary-electron energy distribution and to measure characteristic electron energy-loss spectra. The latter measurements were made for several purposes. First, the loss spectra could be used to determine whether a satisfactory evaporation had been made as the loss spectra for Al, Ni, and Cu are fairly well established.¹ The loss spectrum of Al is simple and easily recognized but the loss spectra for Ni and Cu are more complex. For the latter two metals, it was found convenient to evaporate them (separately) onto a previously evaporated layer of Al to ensure that a sufficiently thick fresh specimen had been produced. The loss spectra were remeasured at frequent intervals during the Auger-electron measurements to monitor possible changes in surface composition. In addition, the loss measurements could be used to establish an absolute energy scale. A relative energy scale was found first by switching batteries (whose emf was determined potentiometrically) successively in series with the voltage sweep. The peak of elastically scattered electrons was thereby moved to different points on the multichannel-analyzer channel scale. The elastic peak locations were determined by computer for the various battery voltages and a quadratic fit was made of the data to determine sweep voltage as a function of channel number; a quadratic relationship was found necessary to account for a small nonlinearity in the multichannel-analyzer output staircase voltage. The absolute electron energy scale, referenced to the Fermi level of the specimen, was established by relating an observed elastic peak position to the voltage applied between the target and the gun cathode with an additive correction of 4.7 eV. This correction includes the thermionic work function of the tungsten cathode (4.5 eV) and the most probable energy of thermionic emission (≈ 0.2 eV for an assumed Maxwellian energy distribution). Auger-electron energies could thus be readily compared with estimates based on electron binding energies (also referenced to the Fermi level).⁸ All energy-loss spectra were measured with incident-electron en-

ergies (at the specimen) close to the energies of interest in the secondary-electron spectra to establish satisfactory operation of the analyzer and to determine the inelastic-scattering modes for the Auger electrons.

Typical voltages applied to the various elements of the apparatus are shown in Table II. All the electrons that were finally detected at the multiplier traversed the analyzer hemispheres with a standard energy of about 10 eV. The energy sweep, applied to elements A2–A12 of the analyzer, had a maximum amplitude of 26 eV for most of the work with Al and of 13 eV for most of the work with Ni and Cu, although occasionally sweeps with larger amplitudes (≈ 45 eV) were used. The smaller sweeps were derived from a more stable amplifier than that used for the larger sweeps and were consistent with the desired energy resolution of 0.1 eV and the channel capacity of the multichannel analyzer.

Secondary-electron data were generally accumulated in 200 channels of the multichannel analyzer at a rate of about 4×10^4 counts/sec. In the work with Ni and Cu, the typical accumulation time for a run was about 8 min (corresponding to $\approx 10^5$ counts/channel), although there were some longer runs of 20–30 min. In the Al work, most of the individual run accumulation times varied between 10 min and several hours, although there were a few ≈ 8 -h runs. The loss spectrum of the sample was measured after each evaporation and each run (measurement time ≈ 30 sec). It is clear that the present samples could have accumulated a monolayer of adsorbed gas during the main data-acquisition periods although it is believed (from the loss spectra) that with frequent evaporations of speci-

TABLE II. Typical voltages applied to the various elements of the scattering apparatus shown in Fig. 1 for the experiments with Al, Ni, and Cu. The symbol S denotes the sweep voltage.

Element	Al	Ni	Cu
G1 (Auger)	-3000	-3000	-3000
(loss)	-1100	-785	-850
G2 (Auger)	-2600	-2600	-2600
(loss)	-880	-640	-700
G3	Ground	Ground	Ground
Specimen	385	Ground	Ground
A1	Ground	Ground	Ground
A2	S (0–26)	S (0–13)	S (0–13)
A3 and A12	-710 + S	-405 + S	-425 + S
A4 and A6	-850 + S	-545 + S	-680 + S
A5 and A10	-1030 + S	-715 + S	-800 + S
A7 and A8	-1090 + S	-775 + S	-840 + S
A9 and A11	-815 + S	-500 + S	-625 + S
A13	45	45	45
A14	Ground	Ground	Ground

men material (to getter the chamber of active gases and to renew the sample surface) and with desorption of adsorbed species by the 3-keV incident-electron beam, no appreciable oxidation or surface reaction was occurring.¹⁵ Some concurrent changes in the energy-loss and Auger spectra were found, however, in the Ni and Cu work, usually either for the first sample of a series of evaporations or over a long period of time (≈ 5 h), and these data will be separately discussed below.

The various individual runs could be combined after calibrations of the energy scales. In the Ni and Cu measurements, the voltages on elements A3–A12 were stepped by intervals of 10 V to cover the energy range of interest. The secondary-electron spectra for each 13-eV sector were summed and combined with neighboring sectors, with appropriate normalizations based on the regions of overlap, to produce the distributions presented below (Fig. 3). These composite spectra were consistent with the distributions obtained with larger sweep amplitudes (≈ 45 eV).

III. RESULTS FOR ALUMINUM

Figure 2 shows a portion of the secondary-electron energy distribution for aluminum in the region

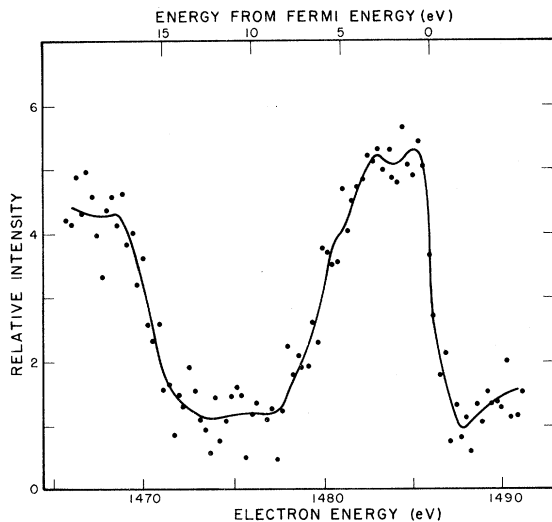


FIG. 2. Portion of the secondary-electron energy distribution for aluminum excited by 3-keV electrons. A quadratic interpolated background has been subtracted from the raw data to display the structure. Each point here represents an accumulation of about 2.9×10^8 counts; the amplitude of the structure is approximately 0.1% of the background intensity. The solid line is a smooth curve (found by a 9-point least-squares cubic-function smoothing procedure) through the experimental points. The Fermi energy has been located at 1485.9 ± 0.5 eV, the point of maximum slope on the high-energy edge of the structure identified as being due to photoemission by internally generated Al $K\alpha_{1,2}$ x rays.

of the expected position of the Al $KL_{2,3}M$ Auger transition. Approximately 145×10^8 counts were accumulated in each channel of the multichannel analyzer (total time ≈ 150 h) but, as the structure is weak, the counts of neighboring pairs of channels were added and a quadratic background (found by interpolation) was subtracted from the raw data to yield the plot of Fig. 2. The peak height of the main structure (located in the vicinity of 1485 eV) is only about 0.1% of the background intensity.

It is well known that Auger electrons emerge from an initially singly ionized atom with energies less than those calculated from ground-state electron binding energies for that atom.¹⁶ For the $KL_{2,3}M$ transition in Al, the Auger feature would be expected¹⁶ to occur with a high-energy edge (corresponding to the Fermi level) at an energy of about 1470 eV. In Fig. 2, however, the main feature with the high-energy edge located at 1485.9 ± 0.5 eV corresponds (within 0.6 eV) to the position of the Al $KL_{2,3}M$ Auger transition calculated with no correction for the atom being left in a doubly ionized state. On energetic grounds, principally, this feature is interpreted¹⁷ as being due to photoexcitation of Al valence electrons by internally generated $K\alpha_{1,2}$ x rays.

At an incident-electron energy of 3 keV, K-shell ionization occurs over a range of depths large compared with the 40-Å attenuation length of 1500-eV electrons in Al.¹⁷ The K-shell fluorescence yield is only 4%, but some of the $K\alpha_{1,2}$ x rays generated deep in the sample can be absorbed in the surface region, close enough to the surface so that a photoelectron can leave the solid without inelastic scattering. The Al $KL_{2,3}M$ Auger transition, however, is weak compared to the KLL transitions¹⁸; in addition, only a small fraction of the Auger electrons resulting from the decay of K vacancies can escape without inelastic scattering. The internal x-ray photoemission peak can thus be expected when the fluorescent yield is not too small. Structure observed at lower energies (shown in Fig. 2 and Ref. 17) is due in part to the expected $KL_{2,3}M$ Auger transition and to inelastic scattering (predominantly multiples of the 15-eV volume-plasmon loss¹⁹) of both photoexcited and Auger electrons.

Baer²⁰ has shown that x-ray photoelectron energy distributions involving valence-band excitation should be simply related to the electronic density of states. The high-energy edge at 1485.9 eV in Fig. 2 then corresponds to the Fermi level of the valence band. The finite width of this edge region is due to the finite analyzer resolution (degraded to 0.2 eV in the data analysis), experimental drifts during data accumulation (estimated to be less than 0.4 eV), and to the spin-orbit splitting of the $K\alpha_{1,2}$ doublet (0.4 eV). The apparent width of the valence band of 8–9 eV is less than the width de-

terminated from soft-x-ray-emission spectroscopy of about 11.3 eV.²¹ This apparent reduction in bandwidth is believed due to a small amount of inelastic scattering; the low-energy portion of the photoelectron band is distorted by 10-eV surface-plasmon losses¹⁹ of photoelectrons of higher energy and it is thus not possible to locate readily the bottom of the band.

The shape of the photoelectron band in Fig. 2 is similar to the calculated Al density of states.²² The experimental distribution is fairly smooth, within the statistical uncertainties, but weak structure is believed detectable at about 3 and 5.6 eV below the Fermi energy. This structure corresponds to symmetry points in the Brillouin zone²² and is similar to that observed by Huen and Wooten²³ in uv photoelectron distributions.¹⁹

IV. RESULTS FOR NICKEL AND COPPER

A. Discussion of Main Data

Figure 3 shows the secondary-electron energy distributions of Ni and Cu in the vicinity of the expected positions of the $L_3M_{2,3}M_{4,5}$ Auger transitions.²⁴ The vertical bars in each panel indicate the positions of the designated Auger transitions expected on the basis of pure $j-j$ coupling.¹⁶ These positions have been computed with the binding energies of Table I and with no correction (estimated to be about -5 to -10 eV) due to the emitting atom being left in a doubly ionized state.¹⁶ We note also that the tabulated binding energies⁸ for the $M_{2,3}$ levels of Ni and Cu are about 2.4 eV higher and 1.0 eV lower, respectively, than the M_3 binding energies derived from recent soft-x-ray-emission ex-

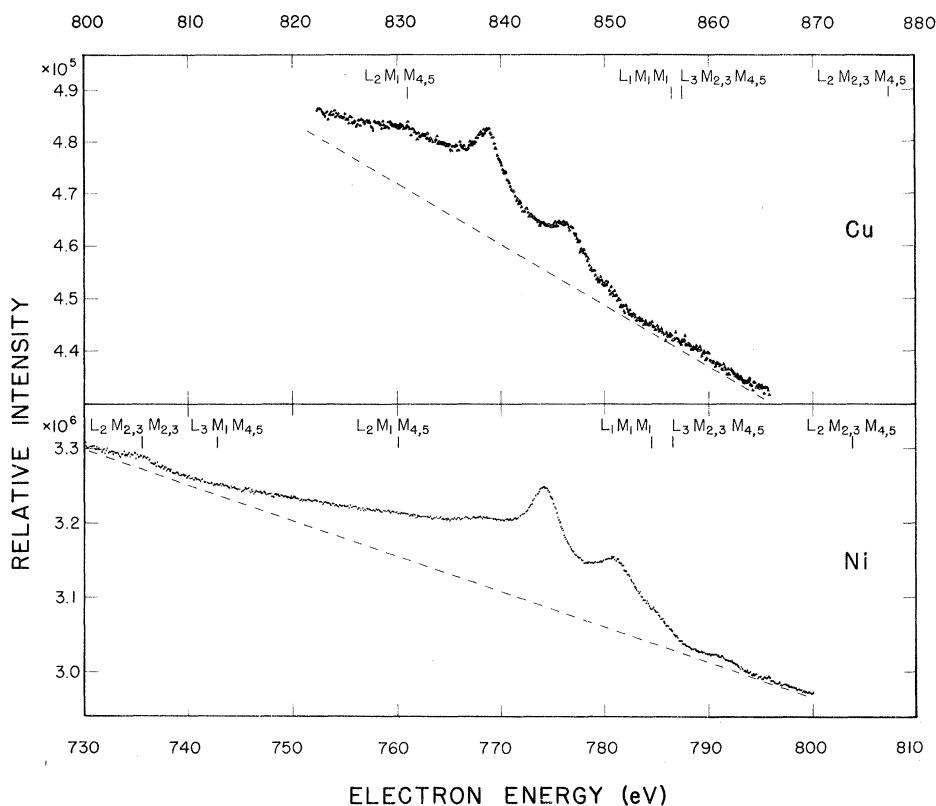


FIG. 3. Portions of the secondary-electron energy distributions for Ni and Cu excited by 3-keV electrons. Many individual runs were obtained, as described in the text, and combined after separate calibrations of the multichannel-analyzer channel scale and conversion of the observed number of counts/channel to number of counts at 0.1-eV intervals (using a local four-channel quadratic fit). The ordinate scale thus corresponds to the number N of accumulated counts per channel; the probable error of a single point is approximately $N^{1/2}$. The dashed lines represent an assumed linear background (to partially compensate for inelastic scattering) to give the curves of Fig. 4. Vertical bars indicate the positions of the particular Auger transitions based on pure $j-j$ coupling and calculated with the electron binding energies shown in Table I. Auger transitions would be expected to be observed at energies about 5–10 eV less than those indicated as the emitting atom is left doubly ionized.

periments.¹⁰

The most prominent feature in each distribution of Fig. 3 is a pair of peaks that has been observed previously.²⁵ These peaks occur, as expected, at energies somewhat less than the computed $L_3M_{2,3}M_{4,5}$ positions. We note here that there does not appear to be any significant x-ray photoemission in Ni and Cu, as for Al. In principle, $L\alpha_{1,2}$ radiation could excite electrons from the $M_{2,3}$ levels and cause structure at the computed $L_3M_{2,3}M_{4,5}$ Auger-transition energies shown in Fig. 1. This lack of observed x-ray photoelectron structure for Ni and Cu is attributed to the small L_3 -shell fluorescent yield ($\approx 0.6\%$)²⁶ and the presence of stronger Auger transitions than in Al.

We will discuss in some detail the prominent structure in Fig. 3 with four components (located between 767.5 and 785.5 eV for Ni and between 830 and 850.5 eV for Cu) and associate it with the $L_3M_{2,3}M_{4,5}$ Auger transition for each element. The weaker structure at higher energies is due to a similar partially overlapping group due to initial ionizations in the L_2 shell. The weak peak at about 735.5 eV for Ni is believed to be due to the $L_3M_1M_{4,5}$ transition; the $L_2M_1M_{4,5}$ transition would be expected to be about 10 times weaker (by analogy with the structure between 765 and 800 eV) and is not detected here. The $L_1M_1M_1$ transition would be expected to be weak and broad compared to the other structure of Fig. 3 on account of the Coster-Kronig transitions.²⁷ Taking into account the systematic errors (noted above) that are believed to exist in the $M_{2,3}$ binding energies listed in Table I, the computed positions of the $L_1M_1M_1$ and $L_3M_{2,3}M_{4,5}$ transitions would nearly coincide for Cu but would be separated by about 4 eV for Ni. The lack of noticeable differences in the relative intensities of the Auger structure for Ni and Cu in Fig. 3 suggests that there is no appreciable intensity associated with the $L_1M_1M_1$ transition.

An interpretation of the structure of Fig. 3 should take into account the following observations and factors.

(i) The separations of the two prominent peaks in the $L_3M_{2,3}M_{4,5}$ Auger groups for Ni and Cu are about 7 eV, as observed earlier²⁵ and discussed recently by Coad.²⁸ These separations are much larger than the differences in the binding energies of electrons in the M_2 and M_3 shells that can be estimated, by extrapolation,⁸ to be about 2 eV. In addition, the two peaks in each spectrum are of roughly equal intensity (taking into account inelastic scattering that will be discussed below) whereas, on the basis of pure $j-j$ coupling, the ratio of the $L_3M_3M_{4,5}$ intensity to the $L_3M_2M_{4,5}$ intensity would be expected²⁶ to be about 5. We note also that the structure of interest in Fig. 3 is distributed over a total range of about 20 eV.

(ii) The two prominent peaks of each distribution have estimated widths of about 3–4 eV that are consistent (taking into account the estimated smearing in the $L_3M_{2,3}M_{4,5}$ Auger transitions of about 0.6 eV, due to the L_3 and M_3 level widths shown in Table I) with the expected $3d$ bandwidths of about 3 eV that have been determined from other experiments.^{7(b),10,29} Some weak fine structure, defined by sequences of points, is believed detectable in Fig. 3, but there does not appear to be a good correlation in the relative positions of the fine structure on the two main peaks for each element. These observations are discussed further in Sec. IV B.

(iii) As for Al, the attenuation length of ≈ 800 eV Auger electrons is expected to be much shorter than the mean depth of L -shell ionizations. The general increase in intensity with decreasing energy seen in Fig. 3 is believed to be due to inelastic scattering of the Auger electrons. The structure of interest can be displayed more clearly by subtracting an arbitrary linear background, represented by the dashed lines in Fig. 3; the results of this partial correction for inelastic scattering are shown in Fig. 4. The weaker peak at lower energy than the main structure of Figs. 3 and 4 (at ≈ 767.5 eV for Ni and at ≈ 830 eV for Cu) was considered as being possibly due to a specific mode of inelastic scattering associated with either of the more intense pair of peaks (at 774.2 and 780.9 eV for Ni, and at 838.8 and 846.4 eV for Cu). Measurements of the energy-loss spectra for each metal, shown in Fig. 5, indicated that no well-de-

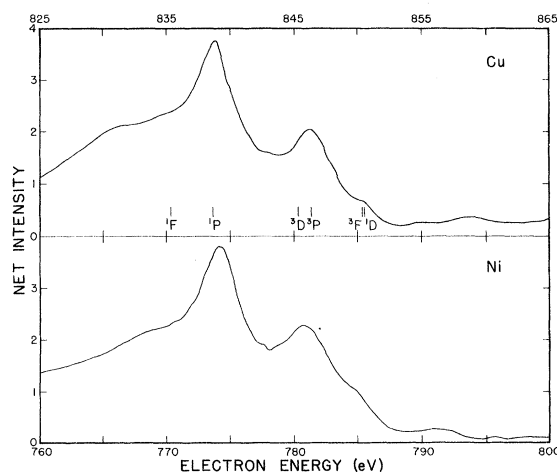


FIG. 4. Smooth curves showing $L_3M_{2,3}M_{4,5}$ and weaker $L_2M_{2,3}M_{4,5}$ Auger transitions for Ni and Cu, obtained by subtracting a linear background from the raw data of Fig. 3, as described in the text. The vertical bars in the top panel denote the calculated relative energy separation of the designated final states for the copper configuration $3s^2 3p^5 3d^9$.

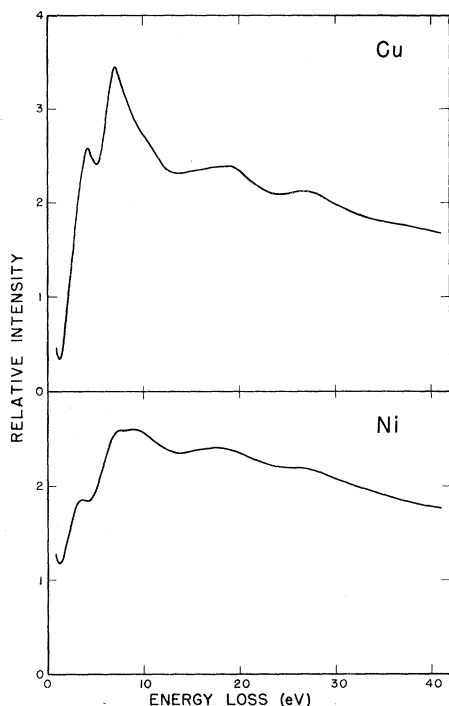


FIG. 5. Energy-loss spectra of Ni and Cu. These spectra were measured with the cathode voltages shown in Table II.

defined inelastic-scattering mechanism could be responsible for the weak 767.5- and 830-eV maxima in Ni and Cu, respectively. It might be remarked that the loss spectra in Fig. 5 are similar to those that have been measured earlier,³⁰ although the structure between 1- and 10-eV energy loss is more prominent in the present data. This increase in relative intensity suggests that this structure is associated with surface-plasmon excitation; the ratio of the intensity due to surface-plasmon excitation to that due to bulk modes of energy loss is known to depend strongly on the surface roughness of evaporated specimens in "reflection" electron-scattering experiments.³¹

(iv) The spectra for Ni and Cu in Fig. 3 are very similar, suggesting a common origin of the structure. The spectra also closely resemble the $L_3 M_{2,3} M_{4,5}$ Auger spectrum of gaseous krypton³² in which a structure consisting of three main peaks and a weaker high-energy component is found. These observations suggest that the principal features of the transition are not a strong function of atomic number and also that the principal transition features do not appear to be appreciably modified, in relative position or intensity, by filling of the 3d level or by solid-state effects.

(v) The Auger spectrum reflects the different possible final states of a system following initial

single ionization of an inner-shell level (that may also be accompanied by additional ionization or excitation).³²⁻³⁴ The more intense features of an Auger spectrum are often due to the "normal" Auger process³³ (decay of a sole inner-shell vacancy) but extra "satellite" features have also been observed with gas samples that can be associated with inner-shell ionization and additional excitation and ionization. We have to consider, for the interpretation of the structure of Fig. 3, whether any of the weaker features (e.g., the shoulders at ≈ 785.5 eV for Ni and ≈ 850.5 eV for Cu, and perhaps the weak structure at higher energy) are Auger satellites, as described. Information on the excitations produced by the incident-electron beam accompanying inner-shell ionization can be obtained from the appropriate x-ray-absorption spectrum.³⁵ Although there is weak structure on the high-energy side of the L_3 absorption edges of Ni and Cu,³⁶ there does not appear to be a satisfactory correlation between these limited data and the weak structure of Fig. 4. This lack of correlation is at first sight surprising as a large majority of the inner-shell ionizations are generally accompanied by excitations of the ejected core electron to states well above ($\gtrsim 10$ eV) the Fermi level (rather than just to states within a few eV of the Fermi level).³⁵ As the ratios of the intensities of the "normal" Auger peaks to the intensities of possible satellite peaks in Fig. 4 are large ($\gtrsim 10$), it can be concluded that the excited core electron is not apparently localized in the vicinity of the core hole or does not significantly contribute to the inner-shell Auger decay process.

(vi) Auger structure due to the $L_2 M_{2,3} M_{4,5}$ transition would be expected at higher energies than the corresponding $L_3 M_{2,3} M_{4,5}$ structure by the amount of the L_2 - L_3 binding-energy difference (17.2 eV for Ni and 19.9 eV for Cu).⁸ On this basis, the peaks at ≈ 791.5 eV for Ni and at ≈ 859 eV for Cu are believed to be the strongest components of the $L_2 M_{2,3} M_{4,5}$ structure, corresponding to the $L_3 M_{2,3} M_{4,5}$ peaks at 774.2 eV for Ni and 838.8 eV for Cu, respectively. We must then consider that some of the intensity in the shoulders located at ≈ 785.5 eV for Ni and ≈ 850.5 eV for Cu is due to a low-energy component of the $L_2 M_{2,3} M_{4,5}$ transitions corresponding to the peaks at ≈ 767.5 eV for Ni and ≈ 830 eV for Cu. Some additional $L_2 M_{2,3} M_{4,5}$ structure would be expected beyond the present range of measurement. The low intensity of the $L_2 M_{2,3} M_{4,5}$ structure relative to the intensity of the $L_3 M_{2,3} M_{4,5}$ structure is believed to be due to the effect of the Coster-Kronig transitions in depleting the number of L_2 -shell vacancies.

The above discussion indicates that pure j - j coupling is inappropriate for a detailed description of the $L_3 M_{2,3} M_{4,5}$ Auger transitions in Ni and Cu.

The structure of Fig. 4 can be qualitatively understood, however, on the basis of L - S coupling and with the use of an atomic model that will be applied, for greater simplicity, only to copper. Following the $L_3M_{2,3}M_{4,5}$ Auger transition, a copper atom would have the configuration $1s^22s^22p^63s^23p^53d^94s$. As noted above, the widths of the principal structure of Fig. 4 reflect mainly the $3d$ bandwidths in each metal and we will ignore here, for simplicity, the $L_3M_{2,3}N_1$ contribution to the Auger spectrum in this energy region as the $4s$ bandwidths are known¹⁰ to be about 9 eV wide and without significant features and as this transition would probably be weaker than the $L_3M_{2,3}M_{4,5}$ transition.²⁷ There are three possible final singlet states (1P_1 , 1D_2 , and 1F_3) and three possible final triplet states ($^3P_{0,1,2}$, $^3D_{1,2,3}$, and $^3F_{2,3,4}$) associated with the $3s^23p^53d^9$ configuration.

Weiss of the NBS has computed the Slater integrals³⁷ based on Clementi wave functions for Cu^{2+} ($3s^23p^63d^9$) in its ground state to enable estimates to be made of the energy differences between the above six final states; these calculated *relative* energy separations are shown in Fig. 4. Additional calculations were made of the final-state energy separations using wave functions for ground-state Cu^+ ($3s^23p^63d^{10}$) and, by extrapolation, ground-state Cu^{3+} ($3s^23p^53d^9$) to determine the extent to which differing atomic wave functions affected the final-state energy separations. The calculated final-state separations for the latter two calculations did not change by more than 1 eV compared to the positions shown in Fig. 4. Although the spin-orbit interaction in the $3p$ shell has been neglected here (splitting ≈ 2 eV) and a simplified atomic model has been used to describe, as a first approximation, an Auger transition involving the valence band of a solid, the calculated Auger-electron energy separations corresponding to the designated final states shown in Fig. 4 agree well with the experimentally observed separations. The largest discrepancy, between the observed peak at ≈ 830 eV and the calculated position corresponding to the 1F state, may not be meaningful but it could indicate that the ≈ 830 -eV peak was a satellite feature as described in item (v) above.

The selection rules for Auger transitions¹⁶ can be applied to indicate that the most intense features of the $L_3M_{2,3}M_{4,5}$ Auger transition would be those corresponding to the 1P and 3P final states.³⁸ For the transition $2p^53p^63d^{10}(^2P) \rightarrow 2p^63p^53d^9\ell$, it is reasonable to presume that the most likely value of ℓ would be zero. In this case, only two 2P terms can be obtained from the $3p^53d^9$ core, one based on the 1P final state and the other based on the 3P state. The separation of the two most intense copper peaks in Fig. 4 corresponds closely to the calculated 1P - 3P final-state energy differ-

ence. The weaker peaks of Fig. 4 may be due to transitions for which $\ell=2$; in this case, 2P terms can be found for all $3p^53d^9$ final states.

We now conclude, on the basis of the above discussion and the calculation of the final-state energy separations for atomic Cu, that the $L_3M_{2,3}M_{4,5}$ Auger structure for Ni and Cu consists of four principal components. Additional weaker structure can be detected in the vicinity of the prominent peaks of Fig. 4 but it is not clear now whether this is due to overlapping final-state components (including possible Auger satellites) or to structure in the density of states (to be discussed below). The calculation for atomic Cu is not expected to be valid in detail for solid Cu while for Ni a greater number of final states (associated with the $3p^53d^8$ configuration) would be possible. In any more detailed analysis, the various final states need to be defined more precisely and appropriate transition probabilities calculated.

B. Density-of-States Information

We will now compare the $L_3M_{2,3}M_{4,5}$ Auger spectra for Ni and Cu with the results of other types of experiments that give information on the valence-band density of states. Figure 6 shows the x-ray photoelectron spectra of Fadley and Shirley^{7(b)} which are similar though not identical to the results of Baer *et al.*²⁹ We also show the

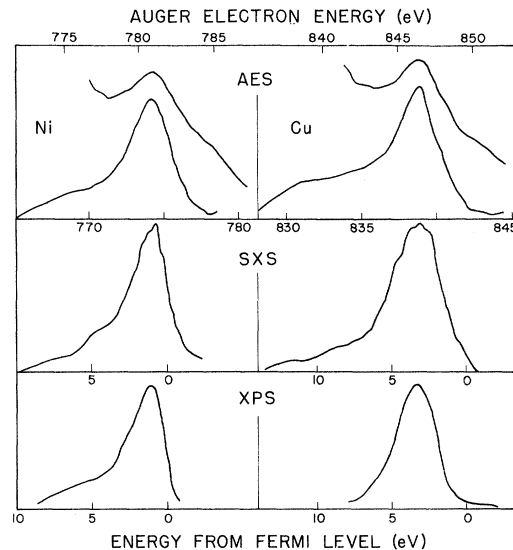


FIG. 6. Comparison of Auger-electron spectra (AES), soft x-ray-emission spectra (SXS) (Ref. 10), and x-ray photoelectron spectra (XPS) [Ref. 7(b)], for Ni (left) and Cu (right). The AES curves have been derived from Fig. 4 with each of the two prominent AES peaks for both Ni and Cu vertically aligned with the SXS and XPS d -band peak positions; the upper and lower AES curves thus correspond to the upper and lower Auger-electron energy scales, respectively, in each panel.

M_3 soft-x-ray-emission spectra of Cuthill *et al.*¹⁰ which show more fine structure than (but which are otherwise similar to) the results of Fomichev *et al.*³⁹ We have not included in this figure uv photoelectron spectra as the measured energy distributions change with photon energy, at least in the 7–40-eV energy range,⁴⁰ although the photoelectron energy distribution^{40(c)} for Ni with $\hbar\omega = 40.8$ eV is similar to the measured x-ray photoelectron spectra.^{7(b),29} The ion-neutralization spectra of Hagstrum⁴¹ have not been included as this technique appears to be more specific to the surface atoms than the “bulk.” The top panels of Fig. 6 show the present Auger data. We have arbitrarily aligned each of the two prominent peaks for each element in Fig. 4 with the $3d$ -band peak positions in the soft-x-ray-emission and x-ray photoelectron spectra in the lower panels of Fig. 6. Unfortunately, the number of final states associated with the $L_3M_{2,3}M_{4,5}$ Auger transitions for Ni and Cu, discussed above, made it difficult to detect any features of the $4s$ bands (associated with the weaker $L_3M_{2,3}N_1$ transitions).

We observe that there is not a close correspondence in the two sections of the Auger-electron spectrum (AES) for each element, as would be expected if each part of the AES could be associated with single final states (well separated in energy). The upper portion of the AES in the top panel is rather broader than the lower portion; this apparent increase in breadth would be expected from the overlapping Auger-electron contributions associated with the 3D and 3P final states indicated for Cu in Fig. 4. It is also believed reasonable to compare data from soft-x-ray spectroscopy (SXS) and x-ray photoelectron spectroscopy (XPS) only with the narrower AES peaks that are more likely to be associated with a single final state (corresponding to the 1P state for atomic Cu).

The lower AES curves are very similar in shape and width to the corresponding SXS and XPS data. Although different electronic processes are involved in each form of valence-band spectroscopy, the similarity in the gross features of the results for each metal suggests that the over-all $3d$ -band characteristics are being measured by each technique with comparable energy resolution. Weak structure is seen in the lower AES curves at the expected positions of the Fermi level but this and the other fine structure, if real, could be associated with overlapping final-state components as well as with structure in the density of states. There does, however, appear to be some correlation between the fine structure in the lower AES curves and that observed in the M_3 soft-x-ray-emission spectra of Cuthill *et al.*¹⁰

The detailed differences in the spectra for each metal in Fig. 6 are considered due to differing in-

itial- or final-state conditions specific to each form of valence-band spectroscopy (assuming that there are no unknown specimen- and measurement-condition artifacts associated with the Fig. 6 data).⁴² Multiple initial- or final-state effects have already been observed in SXS,⁴³ XPS,⁴⁴ and AES (as discussed in Sec. IV A and as evidenced by the maxima at ≈ 767.5 eV for Ni and at ≈ 830 eV for Cu in Fig. 6); multiple final-state effects were not, however, apparent or considered in previous attempts⁶ to derive density-of-states information from AES. Ideally, multiple-state effects and energy-dependent transition probabilities²¹ should be known in a proper analysis of experimental valence-band spectra but, in practice, the necessary corrections cannot usually be determined with the necessary accuracy. It is therefore believed that AES can be a useful complement to SXS and XPS for empirical estimates of the magnitudes of the several possible perturbing effects and for deriving common features of the valence-band density of states.

C. Data for “Contaminated” Ni and Cu Surfaces

It is believed of interest to report briefly some observations of concurrent changes in the energy-loss and Auger spectra of Ni and Cu.

Figure 7 shows the region of the nickel spectrum between ≈ 767 and ≈ 781 eV for what is believed to be a Ni-Al alloy. An apparently thin film of Ni was evaporated onto Al to give the standard Ni loss spectrum [Fig. 5 and curve (a) of Fig. 8]. Auger data were then accumulated for 8 min (with some change in the Auger spectrum over that shown in Fig. 3) and subsequently the data of Fig. 7 were accumulated for a further 15 min. The loss spectrum was remeasured [curve (b) of Fig. 8] and found to be intermediate in appearance between the loss spectra of Ni and Al [curves (a) and (c) of

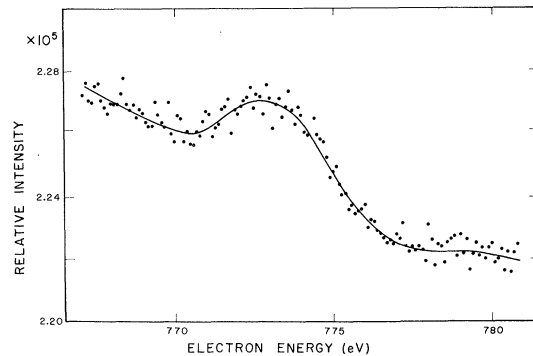


FIG. 7. Nickel Auger structure measured from what is believed to be a Ni-Al alloy (as described in the text). The corresponding characteristic loss spectrum is shown in Fig. 8.

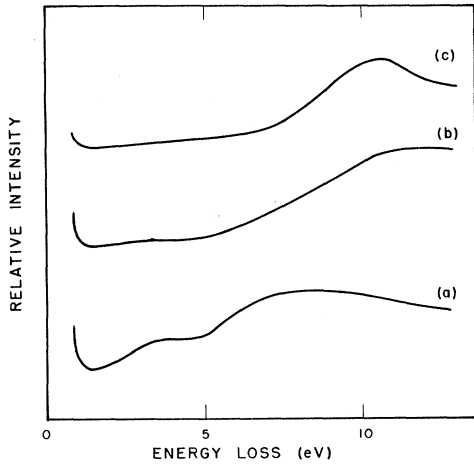


FIG. 8. Characteristic loss spectra of a fresh Ni surface, curve (a), of what is believed to be an Ni-Al alloy, curve (b), and of a fresh Al surface, curve (c). The latter curve shows the 10.3-eV surface-plasmon energy loss.

Fig. 8, respectively]. The Ni Auger signal in Fig. 7 is smaller than for a fresh Ni surface (Fig. 3), and the structure is now centered at a lower energy. Similar observations were made on several occasions. It is believed that aluminum and nickel have

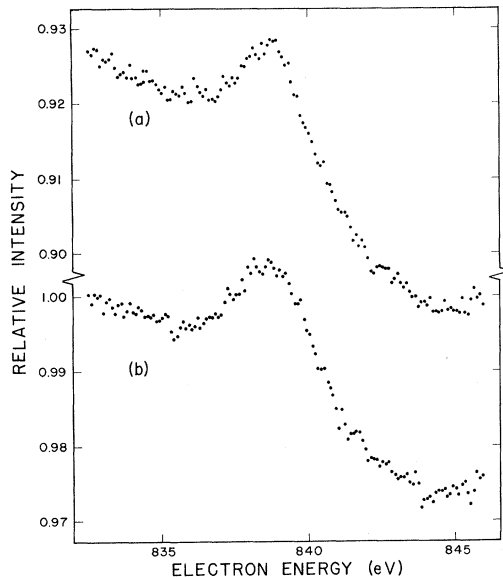


FIG. 9. Copper Auger spectra obtained with a clean surface (data of Fig. 3), curve (a), and with a contaminated surface, curve (b), as described in the text; each point corresponds to an accumulation of about 5×10^5 counts per channel in the multichannel analyzer. These results correspond to the characteristic loss spectra shown in Fig. 10.

interdiffused during the data-accumulation time and that the differences between Figs. 3 and 7 are due to changes in band structures, "chemical" shifts⁴⁵ of the Ni inner-shell energy levels (e.g., the $M_{2,3}$ level), or to a combination of these effects.

Figure 9(a) shows the portion of the copper Auger spectrum between ≈ 833 and ≈ 846 eV (as in Fig. 3). The data shown as Fig. 9(b) were accumulated over a 40-min period beginning 20 min after a copper evaporation. Over this 1-h total period, the characteristic loss spectrum changed as shown in Fig. 10. The changes in the Cu Auger spectrum are small; the main peak has broadened and the fine structure appears to have been smeared out. As for Ni, these changes could be due to Cu-Al interdiffusion or to surface reactions. Changes in the copper loss spectrum were usually apparent only over a period greater than about 5 h after an evaporation. The Auger and characteristic loss spectra of Ni changed concurrently with time qualitatively in the same way as for Cu.

The concurrent changes in the Auger and characteristic loss spectra for Ni and Cu just described clearly indicate the occurrence of chemical changes in the surface regions of the samples. Although the nature of the chemical changes was not identified, it is believed that measurements of Auger-electron spectra (for transitions of the type described here) could yield useful data on changes of densities of states (for example, in alloys, compounds, and with phase changes).

V. SUMMARY

Measurements have been made of selected structure in the secondary-electron energy dis-

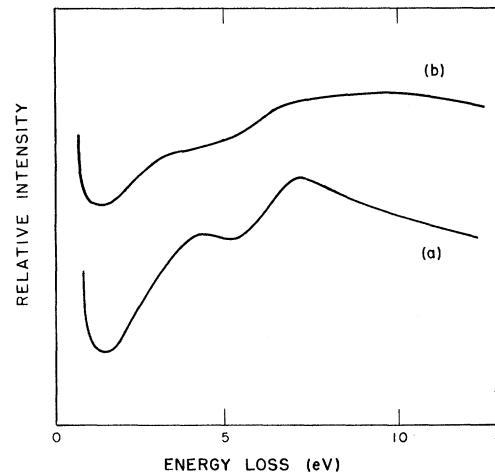


FIG. 10. Characteristic loss spectra of copper measured within a minute of a fresh evaporation, curve (a), and after the surface has become contaminated, curve (b), as described in the text.

tributions of Al, Ni, and Cu. For each element, it was intended to measure a selected Auger transition involving two inner-shell levels and the valence band in order to obtain information about the valence-band density of states.

For aluminum, structure was observed that was interpreted as being due to photoemission of valence-band electrons by internally generated $K\alpha$ x rays. The $KL_{2,3}M$ Auger transition that was originally sought was obscured by inelastic scattering of the photoelectrons. The x-ray photoelectron energy distribution, however, was consistent with uv photoemission data and with density-of-states calculations.

The $L_3M_{2,3}M_{4,5}$ Auger-electron energy distributions in Ni and Cu showed considerable structure, indicating the breakdown of pure $j-j$ coupling. Each transition had four components that could be qualitatively interpreted in terms of the possible final states, expected following the Auger transition, on the basis of an atomic model for Cu. The narrowest component of the structure for each metal (corresponding to a single final state for atomic Cu) was found to be similar in shape to x-ray photoelectron and soft-x-ray-emission spectra

that were obtained with comparable energy resolution. In general, the various possible final states for a given Auger transition need to be explicitly considered before density-of-states information can be extracted from Auger-electron energy distributions.

Some concurrent changes were observed in Auger and characteristic loss spectra for Ni and Cu that could be associated with chemical changes in the surface regions of the samples. It therefore seems likely that changes in the density of states (with compounding, alloying, or phase changes) could be investigated satisfactorily using suitable Auger transitions (that is, with no appreciable overlap of final-state components).

ACKNOWLEDGMENTS

The authors are grateful to Dr. J. W. Cooper and Dr. A. W. Weiss for helpful discussions and for performing the calculations of the final-state splitting for copper. They also wish to thank Dr. J. A. Simpson and Dr. C. E. Kuyatt for the design of the scattering instrument used here and for many other forms of assistance during the course of this work.

*Work carried out at the National Bureau of Standards under the sponsorship of the U. S. Atomic Energy Commission, Division of Biology and Medicine.

[†]Present address: Avco Everett Research Laboratory, Everett, Mass. 02149.

¹H. Raether, Springer Tracts Mod. Phys. **38**, 85 (1965); J. Geiger, *Elektronen und Festkörper, Anregungen, Energieverluste, dielektrische Theorie* (Vieweg, Braunschweig, Germany, 1968).

²N. Swanson and C. J. Powell, Phys. Rev. **167**, 592 (1968).

³R. E. LaVilla and H. Mendlowitz, Phys. Rev. Letters **9**, 149 (1962); J. Daniels, C. V. Festenberg, H. Raether, and K. Zeppenfeld, Springer Tracts Mod. Phys. **54**, 78 (1970).

⁴See, for example, H. Ehrenreich, in *Proceedings of the International School of Physics Enrico Fermi*, edited by J. Tauc (Academic, New York, 1966), Vol. 34, p. 106; M. Cardona, J. Res. Natl. Bur. Std. (U.S.) **74A**, 253 (1970).

⁵J. J. Lander, Phys. Rev. **91**, 1382 (1953).

⁶(a) G. F. Amelio and E. J. Scheibner, Surface Sci. **11**, 242 (1968); (b) G. F. Amelio, *ibid.* **22**, 301 (1970); (c) R. G. Musket and R. G. Fortner, Phys. Rev. Letters **26**, 80 (1971); (d) H. G. Maguire and P. D. Augustus, J. Phys. F **1**, L174 (1971); (e) E. J. LeJeune and R. D. Dixon, J. Appl. Phys. **43**, 1998 (1972).

⁷(a) W. E. Spicer, J. Res. Natl. Bur. Std. (U.S.) **74A**, 397 (1970); (b) C. S. Fadley and D. A. Shirley, *ibid.* **74A**, 543 (1970); (c) G. A. Rooke, *ibid.* **74A**, 273 (1970).

⁸J. A. Bearden and A. F. Burr, Rev. Mod. Phys. **39**, 125 (1967).

⁹L. G. Parratt, Rev. Mod. Phys. **31**, 616 (1959).

¹⁰J. R. Cuthill, A. J. McAlister, M. L. Williams, and

R. E. Watson, Phys. Rev. **164**, 1006 (1967); R. C. Dobbyn, M. L. Williams, J. R. Cuthill, and A. J. McAlister, Phys. Rev. B **2**, 1563 (1970).

¹¹J. R. Pierce, J. Appl. Phys. **11**, 548 (1940).

¹²C. E. Kuyatt and J. A. Simpson, Rev. Sci. Instr. **38**, 103 (1967). The analyzer system used here was functionally similar to that described by G. E. Chamberlain, S. R. Mielczarek, and C. E. Kuyatt [Phys. Rev. A **2**, 1905 (1970)].

¹³The resolution was experimentally established with the analyzer accepting the output of an electron monochromator (Ref. 12) that is not shown in Fig. 1.

¹⁴F. K. Harris, J. Res. Natl. Bur. Std. (U.S.) **13**, 391 (1934); R. H. Lyddane and A. E. Ruark, Rev. Sci. Instr. **10**, 253 (1939).

¹⁵C. J. Powell and J. B. Swan, Phys. Rev. **118**, 640 (1960); C. J. Powell, Australian J. Phys. **13**, 145 (1960).

¹⁶E. H. S. Burhop, *The Auger Effect and Other Radiationless Transitions* (Cambridge U.P., London, 1952); I. Bergström and C. Nordling, in *Alpha-, Beta-, and Gamma-Ray Spectroscopy*, edited by K. Siegbahn (North-Holland, Amsterdam, 1965), Vol. 2, p. 1523.

¹⁷C. J. Powell, Appl. Phys. Letters **20**, 335 (1972).

¹⁸E. J. McGuire, Phys. Rev. **185**, 1 (1969).

¹⁹C. J. Powell, Solid State Commun. **10**, 1161 (1972).

²⁰Y. Baer, Physik Kondensierten Materie **9**, 367 (1969).

²¹G. A. Rooke, in *Soft X-Ray Band Spectra and the Electronic Structure of Metals and Materials*, edited by D. J. Fabian (Academic, New York, 1968), p. 3.

²²N. W. Ashcroft, quoted by F. Wooten, T. Huen, and R. Stuart, in *Proceedings of the International Colloquium on Optical Properties and Electronic Structure of Metals, Paris, 1965*, edited by F. Abelés (North-Holland, Amsterdam, 1966), p. 333; G. A. Rooke, J. Phys. C **1**, 767 (1968); R. Y. Koyama and N. V. Smith, Phys. Rev.

- B 2, 3049 (1970); E. B. Kennard, D. Koskimaki, J. T. Waber, and F. M. Mueller, in *Electronic Density of States*, edited by L. H. Bennett, U. S. Natl. Bur. Std. Spec. Publ. No. 323 (U. S. GPO, Washington, D. C., 1971), p. 795.
- ²³T. Huen and F. Wooten, *Solid State Commun.* 9, 871 (1971).
- ²⁴C. J. Powell and A. Mandl, *Phys. Rev. Letters* 29, 1153 (1972).
- ²⁵S. Aksela, M. Pessa, and M. Karras, *Z. Physik* 237, 381 (1970); J. P. Coad and J. C. Rivière, *ibid.* 244, 19 (1971).
- ²⁶R. W. Fink, R. C. Jopson, H. Mark, and C. D. Swift, *Rev. Mod. Phys.* 38, 513 (1966).
- ²⁷E. J. McGuire, *Phys. Rev. A* 3, 1801 (1971).
- ²⁸J. P. Coad, *Phys. Letters* 37A, 437 (1971). L. Yin, T. Tsang, I. Adler, and E. Yellin [*J. Appl. Phys.* 43, 3464 (1972)] have recently measured the Cu $L_3 M_{2,3} M_{4,5}$ Auger transition and have interpreted their structure with the use of L - S coupling although their assignments differ in some respects from those proposed here.
- ²⁹Y. Baer, P. F. Hedén, J. Hedman, M. Klasson, C. Nordling, and K. Siegbahn, *Phys. Scripta* 1, 55 (1970).
- ³⁰J. L. Robins and J. B. Swan, *Proc. Phys. Soc. (London)* 76, 857 (1960).
- ³¹C. J. Powell, *Phys. Rev.* 175, 972 (1968).
- ³²K. Siegbahn, C. Nordling, G. Johansson, J. Hedman, P. F. Hedén, K. Hamrin, U. Gelius, T. Bergmark, L. O. Werme, R. Manne, and Y. Baer, *ESCA Applied to Free Molecules* (North-Holland, Amsterdam, 1969).
- ³³M. O. Krause, *J. Phys. (Paris) C* 4, 67 (1971); W. E. Moddeman, T. A. Carlson, M. O. Krause, B. P. Pullen, W. E. Bull, and G. K. Schweitzer, *J. Chem. Phys.* 55, 2317 (1971).
- ³⁴H. Körber and W. Mehlhorn, *Z. Physik* 191, 217 (1966); D. Stalherm, B. Cleff, H. Hillig, and W. Mehlhorn, *Z. Naturforsch.* 24a, 1728 (1969).
- ³⁵See, for example, U. Fano and J. W. Cooper, *Rev. Mod. Phys.* 40, 441 (1968).
- ³⁶C. Bonnelle, *Compt. Rend.* 248, 2324 (1959); T. Hayasi, K. Fujimori, and M. Suzuki, *Sci. Rept. Tōhoku Imp. Univ.* 46, 144 (1962); R. J. Liefeld, in *Ref.* 21, p. 133.
- ³⁷E. U. Condon and G. H. Shortley, *The Theory of Atomic Spectra* (Cambridge U. P., London, 1951), Chaps. 7 and 12; J. C. Slater, *Quantum Theory of Atomic Structure* (McGraw-Hill, New York, 1960), Vol. 1.
- ³⁸J. Sugar (private communication).
- ³⁹V. A. Fomichev, A. V. Rudnev, and S. A. Nemnonov, *Fiz. Tverd. Tela* 13, 1234 (1971) [*Sov. Phys. Solid State* 13, 1031 (1971)].
- ⁴⁰(a) D. E. Eastman and J. K. Cashion, *Phys. Rev. Letters* 24, 310 (1970); (b) N. V. Smith and M. M. Traum, *ibid.* 25, 1017 (1970); (c) D. E. Eastman and J. K. Cashion, *ibid.* 27, 1520 (1971).
- ⁴¹H. D. Hagstrum, *J. Res. Natl. Bur. Std. (U.S.)* 74A, 433 (1970).
- ⁴²L. Hedin, B. Lundqvist, and S. Lundqvist, *J. Res. Natl. Bur. Std. (U.S.)* 74A, 417 (1970); H. Ehrenreich, *ibid.* 74A, 293 (1970).
- ⁴³J. W. Cooper and R. E. LaVilla, *Phys. Rev. Letters* 25, 1745 (1970); B. Ekstig, E. Källne, E. Noreland, and R. Manne, *Phys. Scripta* 2, 38 (1970).
- ⁴⁴C. S. Fadley and D. A. Shirley, *Phys. Rev. A* 2, 1109 (1970); P. O. Hedén, H. Löfgren, and S. B. M. Hagström, *Phys. Rev. Letters* 26, 432 (1971); G. K. Wertheim, A. Rosencwaig, R. L. Cohen, and H. J. Guggenheim, *ibid.* 27, 505 (1971).
- ⁴⁵K. Siegbahn, *Phil. Trans. Roy. Soc. London* A258, 33 (1970).

Size Dependence of the Transport Properties of Bismuth in the Phonon-Drag Region

J. - P. Issi and J. H. Mangez

Laboratoire de Physico-chimie et de Physique de l'Etat Solide, Faculté des Sciences Appliquées, Université de Louvain, Louvain, Belgium

(Received 20 July 1972)

The low-temperature size effects in the phonon-drag thermopower and electrical and thermal conductivities of bismuth, measured under identical experimental conditions on a tuning-fork sample of arm thicknesses 2.8 and 1.2 mm, are reported. The thin arm has the highest positive thermopower and a plateau is observed for both thicknesses in a different temperature range. It is shown that the size effect in the thermopower and electrical conductivity occurs in the same temperature range, suggesting that the nonequilibrium phonon distribution should be taken into account in discussing the electrical conductivity at low temperatures. The thermal conductivity exhibits a size effect at temperatures higher than expected.

Throughout the period since the discovery of the peculiar size dependence of the electrical conductivity of bismuth at 4.2 K,¹ its explanation has remained puzzling. The general feature observed^{2,3} is first a decrease of conductivity with thickness, then a leveling off, and then another de-

crease with thickness. Following the observation of phonon-drag humps in the thermopower of bismuth at low temperatures,⁴ one of the present authors (J.-P.I.) suggested that both phenomena might be related.⁵ The electrons dragging the phonons would cause a departure of the phonon